PROCEEDINGS OF SPIE

SPIEDigitalLibrary.org/conference-proceedings-of-spie

Mechanics of flexible electronics and photonics based on inorganic micro- and nanomaterials

Nanshu Lu
Shixuan Yang
Shutao Qiao

SPIE.

Invited Paper

Mechanics of flexible electronics and photonics based on inorganic micro- and nanomaterials

Nanshu Lu[1,*], Shixuan Yang[1], Shutao Qiao[1]

[1]Center for Mechanics of Solids, Structures and Materials, Department of Aerospace Engineering and Engineering Mechanics, Texas Materials Institute, University of Texas at Austin, Austin, TX 78712, USA

ABSTRACT

Flexible electronics and photonics are providing revolutionary solutions for communication, energy, and health care. While some of the organic electronic and photonic materials are intrinsically deformable and low cost to manufacture, their performance and chemical stabilities are yet to match conventional inorganic semiconductors. Strategies for high performance flexible electronics and photonics must overcome challenges associated with the intrinsic stiffness and brittleness of inorganic materials. This paper discusses recent modeling and experimental advancement in the bendability and stretchability of inorganic electronics and photonics. Examples include the discovery of multiple neutral axes in multilayer structures and the comparison between freestanding and polymer-bonded serpentine ribbons.

Keywords: flexible electronics, bendability, stretchability, neutral axis, serpentine

* Correspondence Email: nanshulu@utexas.edu; Phone: +1-512-471-4208; Fax: +1-512-471-3788.

1. Introduction

Research on flexible electronics started nearly two decades ago [1, 2] with the demand of macroelectronics (i.e. large-area electronics), such as paperlike flexible displays [3]. Early research in this area focused on organic semiconductors and conducting polymers because their intrinsic deformability, light weight, and low manufacturing cost are appealing for large-area flexible electronics especially when merged with the roll-to-roll processes [4]. Despite of the

Micro- and Nanotechnology Sensors, Systems, and Applications VI, edited by Thomas George, M. Saif Islam, Achyut K. Dutta, Proc. of SPIE Vol. 9083, 90831J · © 2014 SPIE
CCC code: 0277-786X/14/$18 · doi: 10.1117/12.2051162

merits, difficulties associated with low electronic performance as well as chemical instability have somewhat limited the applications of organic semiconductors in high speed, low power, and long lasting flexible electronics. Advantageously, inorganic semiconductors exhibit high carrier mobility and on-off ratio as well as excellent chemical stability in ambient environments [5]. Furthermore, electronic and mechanical properties of inorganic semiconductors have been well-defined and the manufacturing processes have been well-established after over 100 years of research and applications. As a result, the development of flexible electronics based on rigid yet high-quality monocrystalline inorganic semiconductors started to emerge in the mid-2000s [6].

However, inorganic functional materials such as silicon, glass, and metal are intrinsically stiff, i.e. requiring large force to deform, and often brittle, i.e. cracking at very small strains. To address these fundamental challenges, many mechanics-grounded strategies have been proposed to enable flexible, stretchable, and even bio-integrated electronics based on inorganic functional materials [7]. Successful examples now range from flexible solar cells [8] to stretchable lithium ion battery arrays [9], from bio-inspired electronic eye camera [10] to bio-integrated epidermal electronics [11] and balloon catheters [12].

Although thinning brittle materials down and placing them near the neutral axis are helpful in diminishing bending-induced strains, classical beam theory can be inaccurate in predicting strains in multilayers with large elastic mismatch. Although meandering serpentine structures are found effective in reducing tensile-induced strains, there is no unified theory to predict the strain and compliance of serpentines of different shapes. This paper summarizes our recent modeling and experimental advancement on the bendability (the largest curvature a device can bend) and the stretchability (the largest strain a device can be stretched) of inorganic flexible electronics and it is organized as follows. Section 2 will discuss the bendability of free-standing vs. embedded brittle membranes. Stretchability of freestanding vs. polymer-bonded brittle serpentine ribbons will be discussed in Sections 3 and 4, respectively. Conclusions are offered in Section 5.

2. Bendability of freestanding vs. embedded inorganic films

Basic beam theory predicts that the bending-induced strain in a freestanding membrane is linearly distributed along the thickness direction and the maximum strain ε_b which occurs at the

surface of the membrane is related to the membrane thickness h and the bending radius ρ through the following equation

$$\varepsilon_{\mathrm{b}} = \frac{h}{2\rho} \qquad (1).$$

For a brittle material like silicon, if the allowable maximum strain is limited to a critical value, e.g. $\varepsilon_{\mathrm{cr}} = 1\%$, the maximum allowable bending curvature will be given by

$$\kappa_{\max} = \frac{2\varepsilon_{\mathrm{cr}}}{h} \qquad (2),$$

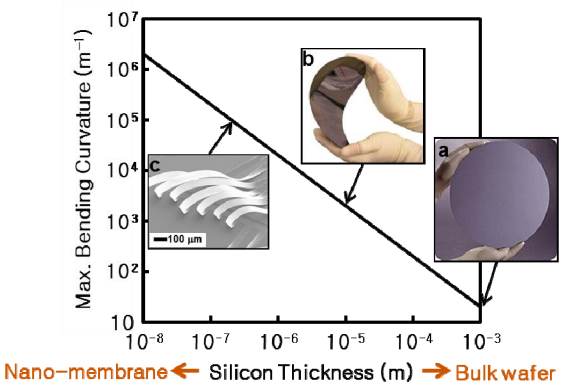

Figure 1 Maximum allowable bending curvature as a function of silicon plate/membrane thickness, with insets showing the bendability of **(a)** a bulk silicon wafer, **(b)** a silicon thin film, and **(c)** silicon nanoribbons.

which is presented as a log-log plot in Figure 1. As the silicon thickness decreases from millimeters to hundreds of nanometers, the attainable bending curvature can increase by four orders of magnitude. As a result, although bulk silicon wafers are rigid plates which are impossible to bend at all (Fig. 1a), silicon thin films become slightly bendable (Fig. 1b) and silicon nanomembranes with thickness on the order of 100 nm can be readily arched to the radius of a folded paper (~0.1 μm) without rupture, as shown in Fig. 1c.

Despite of significant flexibility, freestanding nanomembranes like Fig. 1c are very difficult to handle in practice, plus they need to be integrated into a circuit to be functional. As a result, the brittle nanomembranes are usually embedded in a multilayer stack consisted of both organic and inorganic layers. When a multilayer structure is subject to pure bending, cross-sectional planes are assumed to remain planar after bending in the classical beam theory. Under this assumption, one and only one neutral axis (plane with zero bending strain) can be found for each laminated structure, which is positioned at a distance:

$$b = \frac{\sum_{i=1}^{3} \overline{E}_i h_i \left[\left(\sum_{j=1}^{i} h_j \right) - \frac{h_i}{2} \right]}{\sum_{i=1}^{3} \overline{E}_i h_i} \qquad (3),$$

from the top surface of the stack, where $\overline{E}_i = E_i/\left(1-\nu_i^2\right)$ represents the plane strain modulus with E_i and ν_i being the Young's modulus and Poisson's ratio of each layer (counting from top down), respectively. Hence bending-induced tensile strain can be calculated analytically using:

$$\varepsilon_b = \frac{y}{\rho} \quad (4),$$

where ρ represents the radius of the neutral axis and y is the distance from the point of interest to the neutral axis. Hence strain along the neutral axis is exactly zero and has a linear distribution along the thickness direction.

However, the classical beam theory is only applicable to multilayer stacks with similar Young's modulus. In our recent work on flexible glass photonics as shown in Fig. 2 [13], the Young's modulus of the silicone interlayer is three orders of magnitude smaller than that of SU-8 or polyimide (PI). When this sandwiched "Oreo" structure is subjected to concave bending as shown in Fig. 2a, the silicone middle layer undergoes large shear deformation, which essentially decouples the deformation of the top and bottom stiff layers, similar to the strain decoupling effect discussed in the tension case [14]. As a result, the PI and SU-8 layer each has its own neutral axis and thus the stack demonstrates multiple neutral axes. We validated this postulate using both finite element modeling (FEM) as shown in Fig. 2b and an analytical multi-neutral-axis theory [13], which is compared with Eq. (4) in Fig. 2c. It is evident that the classical beam theory represented by the green curve cannot capture the strain distribution in our multilayer flexible chip and there is one neutral axis in PI and one in SU-8, respectively. Moreover, by tuning the thickness of SU-8, the location of the neutral axis can be shifted (Fig. 2d).

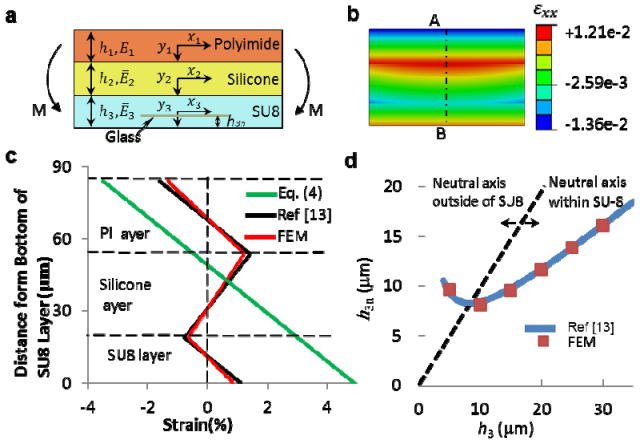

Figure 2 Multiple neutral axes can exist in multilayer stacks with large elastic mismatch. **(a)** Cross-sectional schematic of the flexible photonic chip, with a PI-silicone-SU8 three-layer structure (not drawn to scale), thickness and plane strain modulus are as labeled, and the local coordinate from the median plane of each layer. **(b)** Contour plots of bending strain distribution from FEM when the structure in Fig. 2a is bent concavely. **(c)** Through-stack strain distribution in the flexible chip with the green curve plotted from Eq. (4), the black plotted from analytical results in Ref [13], and the red curve plotted from FEM output. **(d)** The position of SU-8 neutral axis from SU-8 bottom surface as a function of SU-8 thickness. The blue curve comes from analytical results in Ref [13] and the solid markers are FEM results.

The presence of multiple neutral axes offers multiple planes to embed functional brittle materials like silicon and photonic glass in a multilayer laminate, a salient feature which has not been captured by classical beam theory.

3. Stretchability of Freestanding Serpentine Ribbons

While bendability is critical for flexible or rollable electronics, high stretchability and compliance are a must for expandable and bio-integrated electronics. To enable stretchable electronics based on intrinsically unstretchable inorganics, a prevailing strategy is to replace linear films by serpentine ribbons. The stretchability of an island-interconnected-by-serpentine network can vary from 10% to 300% depending on the serpentine geometry [9, 11, 12]. Later, filamentary serpentine network without rigid islands at the intersection nodes has been employed in bio-integrated electronics due to their compliance and conformability to curvilinear tissue surfaces [11, 15]. Besides stretchable electronics, serpentine structures can also be found in a lot of expandable systems made out of intrinsically stiff materials. Examples include the cardiovascular stents for angioplasty [16] or percutaneous coronary intervention [17], and deployable sensor networks for structural health monitoring [18].

Although serpentines have been widely used as the stretchable configuration of stiff materials, the design of the serpentine shape is largely empirical. A few experiments and FEM have been conducted to provide insights into the shape-dependent mechanical behavior [19-21] of serpentine ribbons. Two recent theoretical articles provided viable routes to predict the stretchability of buckled serpentines [22] and self-similar serpentines [23], but the shapes of the unit cells are very limited. Moreover, the effective compliance of the serpentine structure and the shape optimization have been rarely discussed. This section focuses on our recent analytical, FEM, and experimental studies on freestanding serpentines and next section on polymer-bonded serpentines.

To initiate the theoretical analysis and optimization of freestanding serpentine ribbons, we start with a two dimensional (2D) plane strain model, which suppresses the out-of-plane buckling deformation [24]. A unit cell of a representative serpentine ribbon is depicted in Fig. 3a, which can be well defined by four geometric parameters: the ribbon width w, the arc radius R, the arc angle α, and the arm length l. A representative FEM result of a stretched serpentine is given in

Fig. 3b which clearly demonstrates that the maximum strain occurs at the inner edge of the arc crest and is only a small fraction of the applied strain. According to the analytical solutions offered in [24], Figs. 3c&d compare the results of elasticity and curved beam (CB) theory with the FEM results in terms of the normalized stiffness and maximum strains, respectively. It is evident that the geometric effects on the serpentine stiffness and the maximum strain go side-by-side, i.e. serpentines with smaller w/R and larger l/R are more compliant and can survive larger applied strains before rupture. When the arm is extremely long, i.e. $l/R = 50$ as depicted in Fig. 3e, only one thousandth of the applied strain is experienced by the serpentine, as shown in Fig. 3f. In fact, this is the mechanism that has enabled the spider-web-like highly deployable sensor network [18].

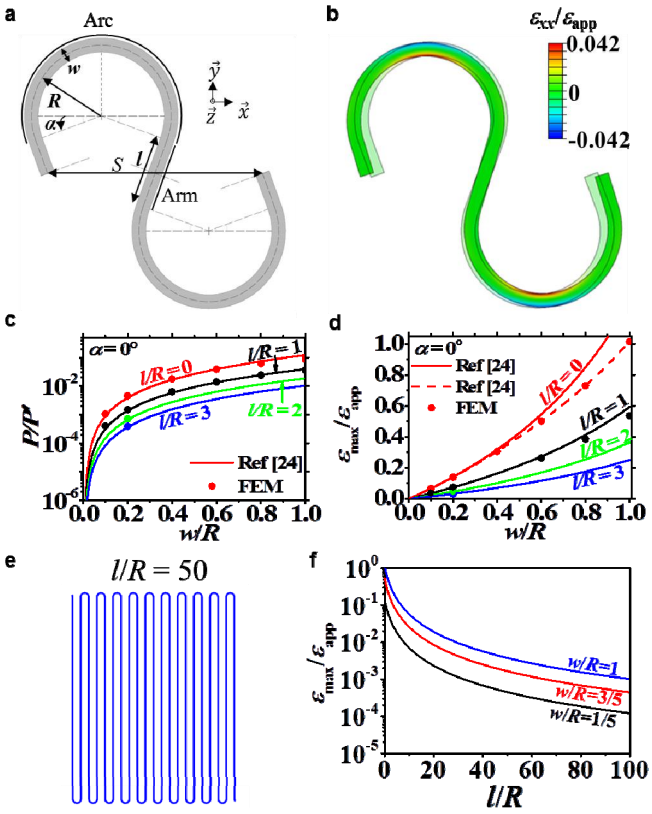

Figure 3 Analytical and FEM results of freestanding serpentines. **(a)** Schematics of a serpentine unit cell where R is the radius of the arc median, w is the width, α is the arc angle, l is the arm length, and S is the end-to-end distance of the unit cell. **(b)** Contour plots of strain fields obtained from FEM with the geometric parameters fixed as $\alpha = 20°$, $w/R = 1/5$, $l/R = 1$. **(c) & (d)** normalized stiffness and maximum strain as a function of w/R when $\alpha = 0°$ and l/R is varying according to the curved beam theory (solid curves) and the elasticity theory (dashed curve) obtained in Ref [24]. **(e) & (f)** Strain in serpentines with very long arm lengths.

Comparison between modeling and experimental results is offered in Fig. 4. Figure 4a shows three different sets of 3D printed brittle serpentine specimens with systematically changing shapes. Every specimen shown in this figure has a thickness of 0.1 inch and a ribbon width of 0.039 inch. Because of the thickness to width ratio, the serpentine specimens undergo in-plane deformation during the tensile tests, which is compatible with our plane strain assumption when the models are derived. The measured $\varepsilon_{cr}/\varepsilon_{app}^{cr}$ are compared with the results from the CB theory and the FEM as given by Figs. 4b-d. All three plots show excellent consistency among the three

different results, indicating reliable analytical and FEM solutions are found for freestanding serpentine ribbons.

4. Stretchability of Kapton-Supported Serpentine Ribbons

The mechanical behaviors of polymer-bonded serpentines are expected to be very different from the freestanding ones. The mechanics of polymer-bonded metallic serpentines has been studied extensively through both experimental [19, 21, 25, 26] and theoretical means [20, 22, 23]. However, so far, there is no experimental investigation or unified theory available to reveal the stretchability of brittle serpentine films of various shapes, on any type of polymer substrates.

Thin indium tin oxide (ITO) films have been a popular electrode material in flat panel displays [27] and solar cells [28] attributing to their combined high electrical conductivity and optical transparency. However, ITO is not mechanically favorable in flexible/stretchable electronics due to its brittle nature. Cracks were observed at applied tensile strains around 1% in polymer-supported blanket thin ITO films [29, 30]. Enhancing the stretchability of

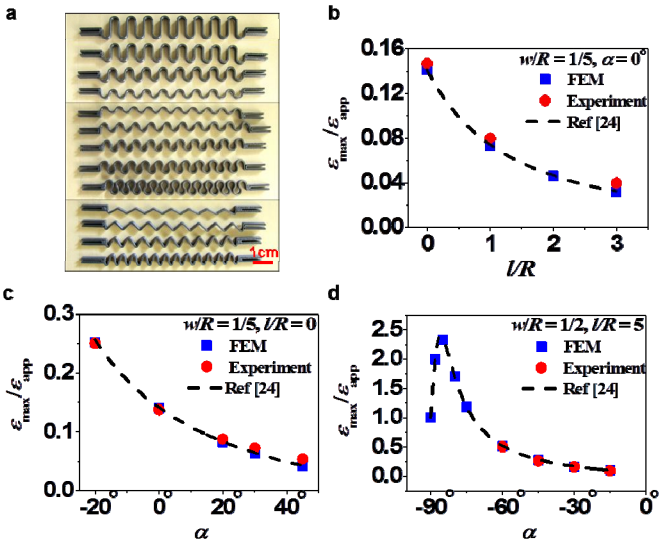

Figure 4 Comparison between modeling and experimental results of freestanding serpentines. **(a)** 3D-printed thick serpentine ribbons to be tested by uniaxial tension. Intrinsic strain-to-rupture of the material, ε_{cr}, is measured using straight specimens. Stretchability, ε_{app}^{cr}, is measured as the applied strain-to-rupture of serpentine specimens. Therefore, experimental $\varepsilon_{cr}/\varepsilon_{app}^{cr}$ should be equivalent to $\varepsilon_{max}/\varepsilon_{app}$ in theory and FEM. Comparison of results from CB theory (dashed curve) in Ref [24], FEM (blue markers), and experiments (red markers) for **(b)** various l/R, **(c)** & **(d)** various α at different w/R.

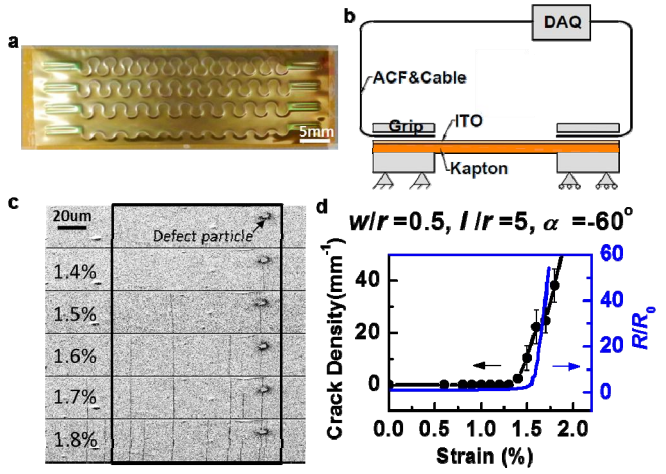

Figure 5 Experimental setup and results of polymer-bonded serpentines. **(a)** Top view of a group of four ITO serpentine thin films sputtered on a 12.7 μm thick Kapton substrate. **(b)** Schematics of the experimental setup for the in situ electrical resistance measurement of the ITO serpentines subjected to uniaxial tension test. **(c)** A sequence of SEM snapshots showing the evolution of crack density with increased applied strain. **(d)** The crack density and electrical resistance of an ITO serpentine as functions of the applied strain. Strains at which the curves blow up are defined as the strain-to-rupture, or stretchability.

thin ITO films bonded on polymer substrates is practically significant for the development of flexible and rollable displays and solar cells.

Resistance vs. applied strain curves have been widely adopted to indicate the stretchability of thin metal [31-33] and ITO films [30]. Our experimental procedures are summarized in Fig. 5 [34]. After taking the ITO coated PI substrate (Kapton) out of the sputter chamber, the straight specimens are cut into long rectangular strips and the serpentine specimens are cut into rectangular pieces each including a group of four or five serpentine ribbons with systematically varied shapes, as shown in Fig. 5a. A schematic of the tension test with *in situ* electrical resistance measurement is shown in Fig. 5b. According to a sequence of scanning electron microscope (SEM) images (Fig. 5c), the correlation between crack density and electrical resistance can be found in Fig. 5d. Despite of the small lag, the resistance is able to capture the failure of the ITO serpentine in a much more experimentally economic way compared to the crack density method.

Experimental, FEM and theoretical results are compared in Fig. 6. A unit cell of the Kapton-supported ITO serpentine subjected to a uniaxial tensile strain, ε_{app}, is depicted in Fig. 6a. Figure 6b offers a representative contour plot of $\varepsilon_{xx}/\varepsilon_{app}$. It is obvious from the strain distribution that the strain concentration always occurs at the inner edge of the arc crest, which is consistent with our experimental observation of preferred crack initiation sites. Similar conclusion has also been drawn from our previous analysis and experiments on freestanding serpentines under plane strain condition [24]. A series of FEMs are performed for systematically varied serpentine shapes. An empirical

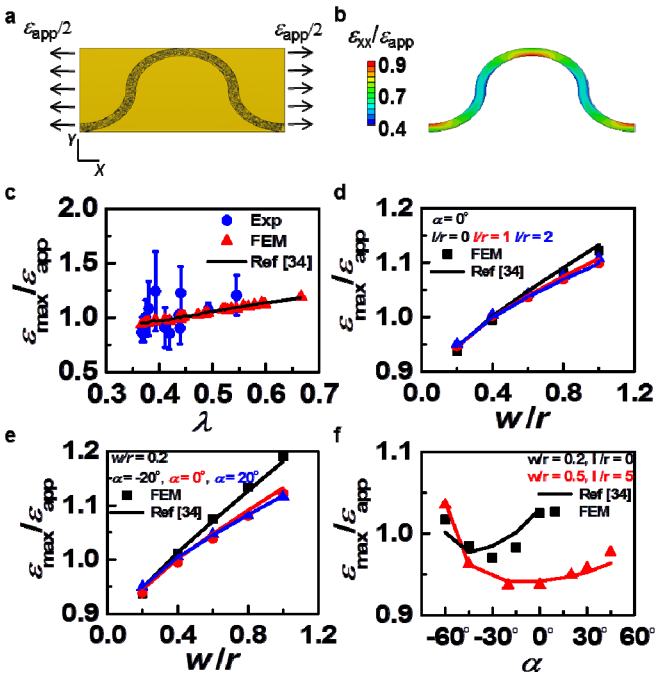

Figure 6 Comparison between experimental and modeling results of polymer-bonded serpentines. **(a)** Boundary condition and **(b)** contour plot of ε_{xx} of a unit cell of a Kapton-bonded ITO serpentine under applied strain ε_{app} = 1%. **(c)** A linear empirical relation obtained in Ref [34] between strain and λ is validated by FEM and experiments. Plots of FEM and empirical equation for **(d)** strain vs. w/r relation with different l/r, **(e)** strain vs. w/r relation with different α, and **(f)** strain vs. α relation with different w/r and l/r.

equation is fitted according to the FEM results as discussed in [34]. The comparison between experiments, FEM, and the empirical equation is given by Fig. 6c. All of the FEM results are able to fall on the linear curve represented by the empirical equation. The experimental data also demonstrates reasonable agreement with limited scatter. This plot is a direct validation of our empirical relation between strain and geometry. Overall, due to the constraint from the stiff Kapton substrate, the geometric effect on serpentine stretchability is much smaller compared to freestanding ones. Figure 6d is plotting $\varepsilon_{max}/\varepsilon_{app}$ as a function of w/r using both the FEM results and the empirical equation. As expected, the empirical equation captures the FEM results very well and w/r always has a monotonic effect on $\varepsilon_{max}/\varepsilon_{app}$. Another important finding is that when w/r is beyond about 0.4, $\varepsilon_{max}/\varepsilon_{app}$ will be beyond 1, which means the stretchability of the serpentine will actually be lower than their straight counterpart, indicating a strain augmentation instead of strain reduction effect. Compared to the effect of w/r, the effects of arm length l/r (Fig. 6d) and α (Fig. 6e) are not as significant, especially when w/r is small. Figure 6f demonstrates the nonmonotonic effect of α on the strains in horseshoe–shaped and V-shaped serpentines. Minimum strains in both types of serpentines occur at some intermediate α values. Again our empirical equation can successfully capture this nonmonotonic dependence attributing to the inclusion of a second order polynomial of w/h.

5. Conclusions

In this paper, we have discussed the rationales behind the emerging configurational strategies to enhance the bendability and stretchability of deformable devices consisted of brittle inorganic materials. For example, adding a soft elastomeric interlayer between stiff polymer layers may induce the split of neutral axis, hence creating more zero-strain planes for the embedment of brittle functional materials for flexible devices. For stretchable devices, the effect of serpentine geometries and substrate constraints are carefully examined. The stretchability of properly designed freestanding serpentines can be thousand times higher than their linear counterpart whereas polymer-bonded serpentines sometimes augment applied strains instead of strain reduction.

Acknowledgement

This work is supported by the NASCENT (Nanomanufacturing Systems for Mobile Computing and Mobile Energy Technologies) Center under NSF Grant No. 1160494.

References

[1] Garnier, F., Hajlaoui, R., Yassar, A. and Srivastava, P., "All-Polymer Field-Effect Transistor Realized by Printing Techniques", *Science* 265(5179):1684-1686 (1994).

[2] Bao, Z. N., Feng, Y., Dodabalapur, A., Raju, V. R. and Lovinger, A. J., "High-performance plastic transistors fabricated by printing techniques", *Chemistry of Materials* 9(6):1299-1301 (1997).

[3] Rogers, J. A., Bao, Z., Baldwin, K., Dodabalapur, A., Crone, B., Raju, V. R., Kuck, V., Katz, H., Amundson, K., Ewing, J. and Drzaic, P., "Paper-like electronic displays: Large-area rubber-stamped plastic sheets of electronics and microencapsulated electrophoretic inks", *Proceedings of the National Academy of Sciences of the United States of America* 98(9):4835-4840 (2001).

[4] Forrest, S. R., "The path to ubiquitous and low-cost organic electronic appliances on plastic", *Nature* 428(6986):911-918 (2004).

[5] Service, R. F., "Materials science - Inorganic electronics begin to flex their muscle", *Science* 312(5780):1593-1594 (2006).

[6] Khang, D. Y., Jiang, H. Q., Huang, Y. and Rogers, J. A., "A stretchable form of single-crystal silicon for high-performance electronics on rubber substrates", *Science* 311(5758):208-212 (2006).

[7] Kim, D. H., Lu, N. S., Ghaffari, R. and Rogers, J. A., "Inorganic semiconductor nanomaterials for flexible and stretchable bio-integrated electronics", *Npg Asia Materials* 4:e15 (2012).

[8] Yoon, J., Baca, A. J., Park, S. I., Elvikis, P., Geddes, J. B., Li, L. F., Kim, R. H., Xiao, J. L., Wang, S. D., Kim, T. H., Motala, M. J., Ahn, B. Y., Duoss, E. B., Lewis, J. A., Nuzzo, R. G., Ferreira, P. M., Huang, Y. G., Rockett, A. and Rogers, J. A., "Ultrathin silicon solar microcells for semitransparent, mechanically flexible and microconcentrator module designs", *Nature Materials* 7(11):907-915 (2008).

[9] Xu, S., Zhang, Y. H., Cho, J., Lee, J., Huang, X., Jia, L., Fan, J. A., Su, Y. W., Su, J., Zhang, H. G., Cheng, H. Y., Lu, B. W., Yu, C. J., Chuang, C., Kim, T. I., Song, T., Shigeta, K., Kang, S., Dagdeviren, C., Petrov, I., Braun, P. V., Huang, Y. G., Paik, U. and Rogers, J. A., "Stretchable batteries with self-similar serpentine interconnects and integrated wireless recharging systems", *Nature Communications* 4:1543 (2013).

[10] Ko, H. C., Stoykovich, M. P., Song, J. Z., Malyarchuk, V., Choi, W. M., Yu, C. J., Geddes, J. B., Xiao, J. L., Wang, S. D., Huang, Y. G. and Rogers, J. A., "A hemispherical electronic eye camera based on compressible silicon optoelectronics", *Nature* 454(7205):748-753 (2008).

[11] Kim, D. H., Lu, N. S., Ma, R., Kim, Y. S., Kim, R. H., Wang, S. D., Wu, J., Won, S. M., Tao, H., Islam, A., Yu, K. J., Kim, T. I., Chowdhury, R., Ying, M., Xu, L. Z., Li, M., Chung, H. J., Keum, H., McCormick, M., Liu, P., Zhang, Y. W., Omenetto, F. G., Huang, Y. G., Coleman, T. and Rogers, J. A., "Epidermal Electronics", *Science* 333(6044):838-843 (2011).

[12] Kim, D. H., Lu, N. S., Ghaffari, R., Kim, Y. S., Lee, S. P., Xu, L. Z., Wu, J. A., Kim, R. H., Song, J. Z., Liu, Z. J., Viventi, J., de Graff, B., Elolampi, B., Mansour, M., Slepian, M. J., Hwang, S., Moss, J. D., Won, S. M., Huang, Y. G., Litt, B. and Rogers, J. A., "Materials for multifunctional balloon catheters with capabilities in cardiac

electrophysiological mapping and ablation therapy", *Nature Materials* 10(4):316-323 (2011).
[13] Li, L., Lin, H., Qiao, S., Zou, Y., Danto, S., Richardson, K., Musgraves, J. D., Lu, N. and Hu, J., "3-D Integrated Flexible Glass Photonics", *Nature Photonics* (2014).
[14] Sun, J. Y., Lu, N. S., Yoon, J., Oh, K. H., Suo, Z. G. and Vlassak, J. J., "Inorganic islands on a highly stretchable polyimide substrate", *Journal of Materials Research* 24(11):3338-3342 (2009).
[15] Yeo, W.-H., Kim, Y.-S., Lee, J., Ameen, A., Shi, L., Li, M., Wang, S., Ma, R., Jin, S. H., Kang, Z., Huang, Y. and Rogers, J. A., "Multi-Functional Electronics: Multifunctional Epidermal Electronics Printed Directly Onto the Skin (Adv. Mater. 20/2013)", *Advanced Materials* 25(20):2772-2772 (2013).
[16] Beyar, R., Roguin, A., Hamburger, J., Saaiman, A., Bartorelli, A. L., DiMario, C., Colombo, A., Hamm, C. W., White, C. J., Marco, J. and Serruys, P. W., "Multicenter pilot study of a serpentine balloon-expandable stent (beStent(TM)): Acute angiographic and clinical results", *Journal of Interventional Cardiology* 10(4):277-286 (1997).
[17] Roguin, A., Grenadier, E., Peled, B., Markiewicz, W. and Beyar, R., "Acute and 30-day results of the serpentine balloon expandable stent implantation in simple and complex coronary arterial narrowings", *American Journal of Cardiology* 80(9):1155-1162 (1997).
[18] Lanzara, G., Salowitz, N., Guo, Z. Q. and Chang, F. K., "A Spider-Web-Like Highly Expandable Sensor Network for Multifunctional Materials", *Advanced Materials* 22(41):4643-4648 (2010).
[19] Gray, D. S., Tien, J. and Chen, C. S., "High-conductivity elastomeric electronics", *Advanced Materials* 16(5):393-+ (2004).
[20] Li, T., Suo, Z. G., Lacour, S. P. and Wagner, S., "Compliant thin film patterns of stiff materials as platforms for stretchable electronics", *Journal of Materials Research* 20(12):3274-3277 (2005).
[21] Hsu, Y. Y., Gonzalez, M., Bossuyt, F., Axisa, F., Vanfleteren, J. and De Wolf, I., "In situ observations on deformation behavior and stretching-induced failure of fine pitch stretchable interconnect", *Journal of Materials Research* 24(12):3573-3582 (2009).
[22] Zhang, Y. H., Xu, S., Fu, H. R., Lee, J., Su, J., Hwang, K. C., Rogers, J. A. and Huang, Y. G., "Buckling in serpentine microstructures and applications in elastomer-supported ultra-stretchable electronics with high areal coverage", *Soft Matter* 9(33):8062-8070 (2013).
[23] Zhang, Y., Fu, H., Su, Y., Xu, S., Cheng, H., Fan, J. A., Hwang, K.-C., Rogers, J. A. and Huang, Y., "Mechanics of ultra-stretchable self-similar serpentine interconnects", *Acta Materialia* 61(20):7816-7827 (2013).
[24] Widlund, T., Yang, S., Hsu, Y.-Y. and Lu, N., "The Stretchability and Compliance of Freestanding Serpentine-Shaped Ribbons", *International Journal of Solids and Structures* submitted (2014).
[25] Hsu, Y. Y., Gonzalez, M., Bossuyt, F., Vanfleteren, J. and De Wolf, I., "Polyimide-Enhanced Stretchable Interconnects: Design, Fabrication, and Characterization", *Ieee Transactions on Electron Devices* 58(8):2680-2688 (2011).
[26] Kim, D. H., Song, J. Z., Choi, W. M., Kim, H. S., Kim, R. H., Liu, Z. J., Huang, Y. Y., Hwang, K. C., Zhang, Y. W. and Rogers, J. A., "Materials and noncoplanar mesh designs for integrated circuits with linear elastic responses to extreme mechanical deformations",

Proceedings of the National Academy of Sciences of the United States of America 105(48):18675-18680 (2008).

[27] Betz, U., Olsson, M. K., Marthy, J., Escola, M. F. and Atamny, F., "Thin films engineering of indium tin oxide: Large area flat panel displays application", *Surface & Coatings Technology* 200(20-21):5751-5759 (2006).

[28] Schmidt, H., Flugge, H., Winkler, T., Bulow, T., Riedl, T. and Kowalsky, W., "Efficient semitransparent inverted organic solar cells with indium tin oxide top electrode", *Applied Physics Letters* 94(24) (2009).

[29] Leterrier, Y., Medico, L., Demarco, F., Manson, J. A. E., Betz, U., Escola, M. F., Olsson, M. K. and Atamny, F., "Mechanical integrity of transparent conductive oxide films for flexible polymer-based displays", *Thin Solid Films* 460(1-2):156-166 (2004).

[30] Mani, G., Feldman, M. D., Patel, D. and Agrawal, C. M., "Coronary stents: A materials perspective", *Biomaterials* 28(9):1689-1710 (2007).

[31] Lu, N. S., Wang, X., Suo, Z. and Vlassak, J., "Metal films on polymer substrates stretched beyond 50%", *Applied Physics Letters* 91(22):221909 (2007).

[32] Niu, R. M., Liu, G., Wang, C., Zhang, G., Ding, X. D. and Sun, J., "Thickness dependent critical strain in submicron Cu films adherent to polymer substrate", *Applied Physics Letters* 90(16) (2007).

[33] Lu, N. S., Suo, Z. G. and Vlassak, J. J., "The effect of film thickness on the failure strain of polymer-supported metal films", *Acta Materialia* 58(5):1679-1687 (2010).

[34] Yang, S., Su, B., Bitar, G. and Lu, N., "Stretchability of indium tin oxide (ITO) serpentine thin films supported by Kapton substrates", *Journal of Materials Research* submitted (2014).